JOURNAL OF SPACECRAFT AND ROCKETS
Vol. 42, No. 2, March–April 2005

2005 Version of the Aeroprediction Code (AP05)

F. G. Moore*
Aeroprediction, Inc., King George, Virginia 22485
and
T. C. Hymer†
U.S. Naval Surface Warfare Center, Dahlgren, Virginia 22448

A new version of the aeroprediction code (APC), the AP05, has been developed. The AP05 addresses additional emerging projectile and weapon needs not met by the former version of the APC, the AP02, along with providing additional productivity and user flexibility options. Some of the new elements of the AP05 include three-fin aerodynamics capability, trailing-edge wing bluntness effects on normal force coefficient, truncated fin leading-edge and body-nose bluntness improvements on axial force coefficient, improved two-dimensional base pressure coefficients for fins, and small caliber weapons capability. Some of the improved productivity and user flexibility options include trim aerodynamics, protuberance aerodynamics input options, increase in altitude limits for trajectory simulations, and user-defined boundary-layer transition for the body and wing. In addition, several errors in the AP02 were corrected for the AP05. Approximately 50 cases were considered for comparing the AP05 aerodynamic predictions to the AP02 and experimental data. It was found that the AP05 gave improved accuracy over the AP02 compared to the experiment for those areas where new elements had been incorporated into the AP02 to form the AP05 and where errors in the AP02 were corrected. However, for those cases where the new elements of the AP05 were not utilized, similar accuracy of the AP02 and AP05 codes compared to experimental data was seen. Several of the new elements of the AP05 were seen to improve productivity substantially over the AP02, the most significant being the automation of trim aerodynamics. The AP05 is, thus, the most accurate and robust of the APCs produced to date.

Nomenclature

A_{BLE}	=	area of blunt portion of wing leading edge, ft^2
A_P	=	planform area of body in crossflow plane, ft^2
A_{ref}	=	reference area (maximum cross-sectional area of body, if a body is present, or planform area of wing, if wing along), ft^2
AR	=	aspect ratio
C_A	=	axial force coefficient
C_{A_B}, C_{A_F}, C_{A_W}	=	base, skin-friction, and wave components, respectively, of axial force coefficient
C_{A_W}	=	axial force of wings
$(C_A)_{\text{SF}}$, $(C_A)_{\text{SW}}$	=	axial force coefficient of a single fin or wing, respectively
C_D	=	drag coefficient
C_{d_c}	=	crossflow drag coefficient
C_L	=	lift coefficient
C_{L_α}	=	lift coefficient derivative, per radian
$(C_{L_\alpha})_0$, $(C_{N_\alpha})_0$	=	lift coefficient or normal force coefficient derivative, respectively, with sharp trailing-edge fins, per radian
C_{ℓ_P}	=	roll damping moment coefficient
C_M, ΔC_M	=	pitching moment coefficient or change in pitching moment coefficient (based on reference area and body diameter, if body present, or mean aerodynamic chord, if wing alone)
C_{M_B}	=	pitching moment coefficient of body alone
$C_{M_{B(W)}}$, $C_{M_{W(B)}}$	=	pitching moment coefficient of body in presence of wing or wing in presence of body
$C_{M_q} + C_{M_{\dot\alpha}}$	=	pitch damping moment coefficient, $[C_M(q)/(qd/2V_\infty) + C_M(\dot\alpha)/(\dot\alpha d/2V_\infty)]$
C_{M_α}, ΔC_{M_α}	=	pitching moment coefficient derivative or change in pitching moment coefficient derivative, per radian
$(C_{M_\alpha})_0$	=	pitching moment coefficient derivative for sharp trailing edge fins, per radian
C_N, ΔC_N	=	normal-force coefficient or change in normal-force coefficient
C_{N_B}	=	normal-force coefficient of body alone
$C_{N_{B(W)}}$, $C_{N_{B(T)}}$	=	normal-force coefficient on body in presence of wing or tail
C_{N_W}	=	normal-force coefficient of wing alone
$C_{N_{W(B)}}$, $C_{N_{F(B)}}$	=	normal-force coefficient of wing or fin in presence of body
C_{N_α}, ΔC_{N_α}	=	normal-force coefficient derivative or change in normal-force coefficient derivative, per radian
$(C_N)_{\text{SW}}$	=	normal-force coefficient of single wing (two fins)
C_P, C_{P_0}	=	pressure and stagnation pressure coefficient
$C_{P_{2\text{-D}}}$	=	two-dimensional base pressure coefficient
c, c_r, c_t	=	local chord, root, and tip chord
d, d_B	=	diameter and body base diameter, ft
d_N	=	diameter of truncated nose tip, ft
d_{ref}	=	reference body diameter, ft
F_6, F_8	=	empirical factors used to represent aerodynamics of six and eight fins based on four-fin aerodynamics
f_1, f_2, f_3, f_4	=	factors used in trailing-edge bluntness methodology
h	=	wing trailing-edge thickness, ft
$K_{B(W)}$, $K_{B(T)}$	=	ratio of additional body normal-force coefficient in presence of wing, or tail to wing, or tail alone normal-force coefficient at $\delta = 0$ deg

Received 30 January 2004; revision received 7 June 2004; accepted for publication 14 June 2004.

*President, 9449 Grover Drive, Suite 201; drfgmoore@hotmail.com. Associate Fellow AIAA.

†Aerospace Engineer, Weapons Systems Department, Missile Systems Division, Dahlgren Division. Member AIAA.

$K_{W(B)}$, $K_{T(B)}$	=	ratio of normal-force coefficient of wing or tail in presence of body to that of wing or tail alone at $\delta = 0$ deg
l	=	length, ft or calibers
M	=	Mach number, freestream Mach number
M_N	=	Mach number normal to body, $M_\infty \sin\alpha$
M_{N_C}	=	normal Mach number to body where flow goes supercritical (assumed to be $M_N = 0.1$ in AP05)
QE	=	launch angle, deg
Re_N	=	Reynolds number
Re_{N_C}	=	crossflow Reynolds number where flow transitions from subcritical to supercritical condition
Re_{N_T}	=	Reynolds number where flow transitions from laminar to turbulent conditions
r_{LE}, r_{TE}	=	leading and trailing-edge radius of wing, ft
r_n	=	body nose tip radius, ft
t, t_r, t_t	=	thickness, root chord, and tip chord thickness of wing, ft
V_∞	=	freestream velocity, ft/s
W	=	weight, lb
X_{CP}	=	center of pressure in x direction, ft or calibers from some reference point that can be specified
X_{CP}/d	=	center of pressure, calibers from some reference point
α	=	angle of attack, deg
γ	=	ratio of specific heats of air
ΔC_{A_W}	=	change in axial force coefficient due to truncated nose tip at subsonic and transonic Mach numbers
ΔM_{N_C}	=	amount the Mach number deviates from the assumed supercritical value of $M_N = 0.1$ in AP05
δ	=	control deflection, positive leading edge up, deg
η	=	ratio of normal force of circular cylinder of given length to diameter ratio to that of a cylinder of infinite length
Φ	=	roll position of missile fins, deg, where 0 deg corresponds to fins in the plus orientation, 45 deg corresponds to fins rolled to the cross orientation

Subscripts

trim	=	denotes conditions where trim occurs so that pitching moment is zero
4f	=	four-fin data

Introduction

THIS This paper documents the new theoretical elements that have been integrated into the 2002 version (AP02) of the aeroprediction code (APC) to form the 2005 version of the APC, the AP05. AP05 is the ninth version of the APC developed. The first three versions of the APC, AP72 (Ref. 1), AP74 (Ref. 2), and AP77 (Ref. 3), were aimed at meeting unguided and guided projectile requirements. The next four versions of the APC, AP81 (Ref. 4), AP93 (Ref. 5), AP95 (Ref. 6), and AP98 (Ref. 7), addressed missile requirements, which tend to fly at higher Mach numbers and angles of attack (AOA) and also to have more general body geometries than projectiles. AP02 (Ref. 8) met many projectile needs that had emerged over about a 25-year period between 1977 and 2002. AP05 addresses several additional projectile and weapon needs along with continuing to improve productivity and making the APC more robust. Table 1 summarizes the historical evolution of the APC.

The additional projectile and weapon needs mentioned earlier include three-fin aerodynamics, trailing-edge bluntness effect on normal force and center of pressure, and ability to compute accurate aerodynamics on small diameter weapons (as small as 1-mm diameter). In addition, improved axial force accuracy for all weapons that have truncated noses or truncated leading or trailing edges was accomplished through development of improved methodology. Improved productivity was obtained by generating trim aerodynamics, by allowing user inputs for protuberance aerodynamics and Reynolds number for boundary-layer transition, and by modifying the trim trajectory option to fly at higher altitude than allowed in the AP02. Finally, the code interface has been extended to operate on Windows XP software along with Windows 98, 2000, and NT. Therefore, it is believed the AP05 is the most accurate and robust of the APCs produced to date.

This paper will discuss the new theoretical elements added to the AP02 to form the AP05. A single example will then be chosen to illustrate each of the new methods. For those interested in more examples or more detailed derivation of the new methods, Ref. 9 should be consulted.

AP05 New Capability

Each of the new elements of the AP05 mentioned in the Introduction will be briefly discussed in this section of the paper.

Three-Fin Aerodynamics

The multifin aerodynamics considered for the AP02 was to add six- and eight-fin capability to the existing two- and four-fin capability of the AP98. Since that time, several agencies have asked about three-fin aerodynamics capability. The applications for the three-fin configurations are rockets, flechettes, and other lower cost unguided ordnance. As a result of this need, three-fin aerodynamic capability will be a part of the AP05.

To compute aerodynamics of configurations that have three fins, slender-body-theory (SBT) will be used for low AOA. An extension of the factors computed by computational fluid dynamics codes for six- and eight-fin cases[10] will be extended to three fins for high AOA.

Figure 1 shows SBT applied to a wing–body or body–tail case. Refer to Fig. 1: It is seen that triform missiles exhibit roll independence of aerodynamics at low AOA just like cruciform missiles. It is also seen that the axial force, normal force, pitching moment, and pitch damping moment coefficient for triform missiles is equal to the body alone plus three-quarters of the cruciform wing alone or wing plus interference effects as is appropriate. The roll damping is equal to that of the body alone plus 80% of the cruciform fin value.

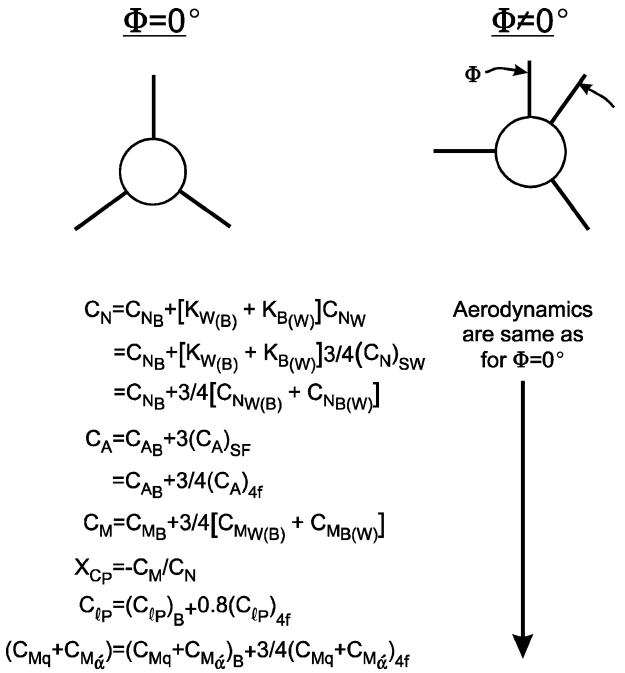

Fig. 1 Aerodynamics of triform body tail at low AOA as a function of roll.

Table 1 Evolution of APC in terms of major new added capability

Version	Weapons	Aero-dynamics	Flight conditions: Mach No.	Real gas available	AOA range, deg	Roll, deg	Trajectory available	Nonlinear distributed loads available	Computers	Emerging projectile needs	Trim aero-dynamic outputs
1972	Axisymmetric unguided projectiles	Static only	0–3	No	0–15	$\Phi = 0$	No	No	CDC	No	No
1974	Axisymmetric unguided projectiles, rockets, missiles	Same	0–3	No	Same	Same	No	No	CDC	No	No
1977	Same	Static and dynamic	0–3	No	Same	Same	No	No	CDC, IBM	No	No
1981	Same	Same	0–8	No	0–15 (limited configurations at higher α)	Same	No	No	CDC, IBM, VAX	No	No
1993	Same	Same	0–20	Yes	0–30	Same	No	No	CDC, IBM, VAX Silicon Graphics	No	No
1995	Same	Same	Same	Yes	0–90	Same	No	No	Interactive personal computer	No	No
1998	Axisymmetric and asymmetric missiles, rockets	Same	Same	Yes	Same	$\Phi = 0, 45$	No	Yes	Interactive personal computer Windows 98 only	No	No
2002	Same plus 6, 8 fin	Same	Same	Yes	Same	Same	Yes	Yes	Improved interactive personal computer, Windows 98, 2000, and NT	Yes	No
2005	Same plus 3 fin	Same	Same	Yes	Same	Same	Yes with altitude increase	Yes	Same plus Windows XP	Yes plus additional capability	Yes

At high AOA, triform fins are assumed to have the $\cos^2 30\ \text{deg} = 0.75$ factor applied to the cruciform values of wing–body and body–wing interference effects as well. In other words, at high AOA, the factors in Fig. 1 are applied to the cruciform fin aerodynamics.

The way the triform aerodynamics are computed in the AP05 is as follows:

1) Compute aerodynamics of a cruciform body–tail configuration identical to the triform case except we have four fins at $\Phi = 0$ deg roll vs three fins.

2) Compute body alone and wing–body interference aerodynamics at the roll, α and M conditions desired.

3) Compute aerodynamics of the triform missile at each α and M from the equations given in Fig. 1

Trailing-Edge Bluntness Effect on Normal Force

The motivation behind incorporating trailing-edge bluntness effects into the APC is driven by the desire to estimate more accurately the normal-force coefficient slope and static stability of guided projectiles at high launch velocities. Many guided projectiles are constrained in length, and with the desire to increase range, any improvements in static stability at high Mach numbers is important. The trailing-edge bluntness effect on low AOA normal-force coefficient has been presented previously,[11] and therefore, the results will only be briefly summarized here for completeness.

In Ref. 12, it was shown that there was a consistent improvement in normal-force coefficient slope of wings at low AOA, with the percent increase in C_{N_α} increasing with increasing supersonic Mach numbers. In Ref. 12 a simple formula is given to estimate the effect of trailing-edge thickness on the lift curve slope with engineering accuracy as

$$C_{L_\alpha} = \left(C_{L_\alpha}\right)_0 [1 + 1.2\,(h/c)] \tag{1}$$

Chapman[12] indicated Eq. (1) was a first approximation to the trailing-edge thickness effects for wings of aspect ratio greater than one, for Mach numbers between 1.5 and 3.1, and for turbulent flow on the wings. The wings that were tested also had a sharp leading edge and were rectangular. Equation (1) basically says that the lift coefficient slope at small AOA for a wing with trailing-edge thickness is increased in a direct proportion to the trailing-edge thickness. For example, for a wing that had a 10% trailing-edge thickness ratio ($h/c = 0.1$), then Eq. (1) says that the C_{L_α} is increased by 12% over a wing with no trailing-edge thickness, $C_{L_\alpha} = 1.12(C_{L_\alpha})_0$.

In Ref. 11 a semi-empirical expression is derived analogous to Eq. (1), but more general and robust in its application, that is,

$$C_{L_\alpha} = \left(C_{L_\alpha}\right)_0 [1 + f_1(h/c, M)\, f_2(r_{\text{LE}}/t) \times f_3(\text{AR})\, f_4(\text{NF})(h/c)/(t/c)] \tag{2}$$

Basically, Eq. (2) is analogous to Eq. (1) if one assumes

$$f_1(h/c, M) = 1.2\,(t/c), \qquad f_2(r_{\text{LE}}/t) = 1.0$$
$$f_3(\text{AR}) = 1.0, \qquad f_4(\text{NF}) = 1.0 \tag{3}$$

Another way to look at Eq. (2) is that the lift of wings with blunt trailing edges will be increased slightly over those of sharp trailing edges. The amount of the increase will be defined by the second term within the bracket of Eq. (2). The amount of the increase in lift (or pitching moment) is a function of not only the trailing-edge thickness, but Mach number, wing aspect ratio, wing leading-edge radius, and number of fins (NF) present. Each of the parameters f_1, f_2, f_3, and f_4 were derived in Ref. 11. The parameter f_1 is defined by Fig. 2, f_2 by Eq. (4), f_3 by Eq. (5), and f_4 by the multifin factors in Table 2 for six and eight fins or Fig. 1 for three fins. For those interested in the details of the derivation of f_1, f_2, f_3, and f_4, Ref. 11 should be reviewed. Thus,

$$f_2 = \left(\frac{1 - 2r_{\text{LE}}}{t}\right) \tag{4}$$

$$f_3(\text{AR}) = 1 - \frac{0.128}{\text{AR}\sqrt{M_\infty^2 - 1}}, \qquad M_\infty \geq 1.2$$

Table 2 Approximated values of the facors F_6 and F_8 obtained from smoothed values of the ZEUS and GASP code computations and engineering judgment

	F_6: Mach number					F_8: Mach number				
α	0.6	1.5	2.0	3.0	4.5	0.6	1.5	2.0	3.0	4.5
					AR = 0.25					
0	1.26	1.37	1.27	1.19	1.22	1.90	1.42	1.40	1.27	1.20
15	1.00	1.00	1.10	1.19	1.35	1.45	1.03	1.17	1.27	1.35
30	1.00	1.00	1.00	1.19	1.22	1.00	1.00	1.01	1.27	1.22
45	1.00	1.00	1.00	1.00	1.00	1.00	1.00	1.00	1.00	1.00
60	1.00	1.00	1.00	1.00	1.00	1.00	1.00	1.00	1.00	1.00
75	1.00	1.00	1.00	1.00	1.00	1.00	1.00	1.00	1.00	1.00
90	1.00	1.00	1.00	1.00	1.00	1.00	1.00	1.00	1.00	1.00
					AR = 0.50					
0	1.35	1.25	1.20	1.30	1.47	2.00	1.36	1.28	1.35	1.72
15	1.06	1.10	1.15	1.29	1.50	1.50	1.18	1.24	1.40	1.83
30	1.00	1.00	1.07	1.29	1.36	1.00	1.08	1.16	1.41	1.60
45	1.00	1.00	1.00	1.00	1.00	1.00	1.00	1.04	1.06	1.20
60	1.00	1.00	1.00	1.00	1.00	1.00	1.00	1.00	1.00	1.00
75	1.00	1.00	1.00	1.00	1.00	1.00	1.00	1.00	1.00	1.00
90	1.00	1.00	1.00	1.00	1.00	1.00	1.00	1.00	1.00	1.00
					AR = 1.0					
0	1.40	1.22	1.35	1.42	1.50	1.92	1.27	1.58	1.96	2.00
15	1.15	1.13	1.23	1.32	1.50	1.69	1.38	1.38	1.80	2.00
30	1.07	1.00	1.00	1.21	1.38	1.43	1.28	1.15	1.64	2.00
45	1.02	1.00	1.00	1.10	1.13	1.20	1.05	1.00	1.48	1.61
60	1.00	1.00	1.00	1.00	1.00	1.00	1.00	1.00	1.32	1.25
75	1.00	1.00	1.00	1.00	1.00	1.00	1.00	1.00	1.16	1.00
90	1.00	1.00	1.00	1.00	1.00	1.00	1.00	1.00	1.00	1.00
					AR = 2.0					
0	1.42	1.50	1.50	1.50	1.50	1.92	1.77	1.97	1.92	1.90
15	1.31	1.41	1.27	1.39	1.50	1.70	1.95	1.75	1.77	2.00
30	1.17	1.00	1.03	1.27	1.45	1.47	1.65	1.57	1.62	2.10
45	1.03	1.00	1.00	1.14	1.23	1.25	1.32	1.27	1.47	1.95
60	1.00	1.00	1.00	1.00	1.00	1.02	1.00	1.02	1.32	1.62
75	1.00	1.00	1.00	1.00	1.00	1.00	1.00	1.00	1.17	1.32
90	1.00	1.00	1.00	1.00	1.00	1.00	1.00	1.00	1.00	1.00
					AR = 4.0					
0	1.50	1.50	1.50	1.50	1.50	2.00	1.90	2.00	2.00	2.00
15	1.33	1.41	1.27	1.39	1.50	1.70	1.95	1.75	1.77	2.00
30	1.17	1.00	1.03	1.27	1.45	1.47	1.65	1.57	1.62	2.00
45	1.03	1.00	1.00	1.14	1.23	1.25	1.32	1.27	1.47	1.95
60	1.00	1.00	1.00	1.00	1.00	1.02	1.00	1.02	1.32	1.62
75	1.00	1.00	1.00	1.00	1.00	1.00	1.00	1.00	1.17	1.32
90	1.00	1.00	1.00	1.00	1.00	1.00	1.00	1.00	1.00	1.00

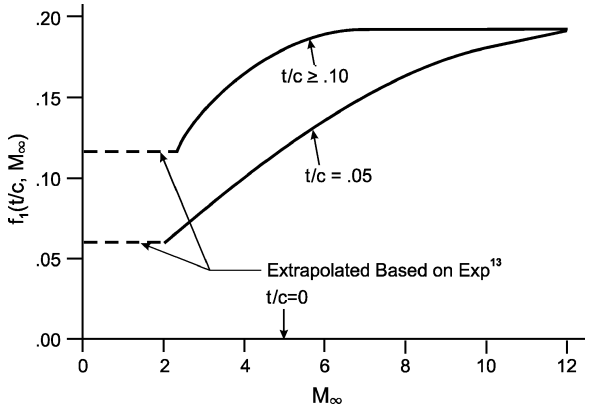

Fig. 2 Parameter used to define the additional normal force increment of a wedge compared to a double wedge airfoil.

$$f_3(\mathrm{AR}) = 1, \qquad M_\infty \le 0.8$$

$$f_3(\mathrm{AR}) = (f_3)_{M=0.8} + \frac{M_\infty - 0.8}{0.4}\left[(f_3)_{M=1.2} - (f_3)_{M=0.8}\right], \qquad 0.8 < M_\infty < 1.2 \tag{5}$$

Substituting Eqs. (4) and (5) into Eq. (2) along with use of Fig. 2 and Table 2 allows one to calculate an approximate value of increase in the low AOA normal-force coefficient of fins. Again $(C_{N_\alpha})_0$ of Eq. (2) is the flat plate, wing-alone value from the AP05, and f_1 is defined by interpolation using given wing parameters and Fig. 2. Equation (2) is the final expression to incorporate wing trailing-edge thickness effects into the low AOA wing lift curve slope.

The AP05 uses a fourth-order method to predict the wing normal force as a function of AOA, Mach number, aspect ratio, and taper ratio. The value of $(C_{N_\alpha})_{\alpha\approx 0}$ is one of the parameters used in the fourth-order method, but it has increasingly less importance as AOA gets larger than 15–20 deg.

In Refs. 12–14, it is shown that there was little change in the wing alone center of pressure due to wing trailing-edge thickness. Because the center of pressure of the wing alone is simply the pitching moment divided by the normal force, the implication is that wing trailing-edge bluntness affects the pitching moment similar to the normal force. Therefore, the wing-alone pitching moment of the AP05 will be modified exactly as follows for trailing-edge bluntness effects, that is,

$$C_{M_\alpha} = (C_{M_\alpha})_0 \left[1 + f_1(h/c, M)\, f_2(r_{\mathrm{LE}}/t) \times f_3(\mathrm{AR})\, f_4(\mathrm{NF})\, (h/c)\,/(t/c)\right] \tag{6}$$

The effect of Eqs. (2) and (6) on the overall configuration aerodynamics will, thus, be to add a slight amount of normal-force and pitching moment coefficient to a wing with blunt trailing edges, particularly for small AOA. If this wing is located at the rear of the configuration, it will have a stabilizing effect on the vehicle. This

stabilizing effect will be the strongest at the higher Mach numbers. On the other hand, if the wing is at the front of the vehicle, the effect will be destabilizing.

Truncated Fin Leading-Edge Axial Force Improvements

In investigating the accuracy of the AP02 compared to experimental data, it was found that fins that had truncated leading edges gave axial-force accuracy problems for Mach numbers less than 1.2. As a result of the need for improved axial force accuracy for truncated leading edge fins, an approximate method was derived.

An approximate method to account for the axial force coefficient on the truncated leading edge of a wing is given by

$$C_{A_{\mathrm{LE}}} = 0.5 C_{P_0}(A_{B\mathrm{LE}}/A_{\mathrm{ref}}) \tag{7}$$

C_{P_0} of Eq. (7) can be approximated from

$$C_{P_0} = \left(2/\gamma M_\infty^2\right)\left[\left\{1 + [(\gamma - 1)/2]M_\infty^2\right\}^{\gamma/(\gamma-1)} - 1\right] \tag{8}$$

$A_{B\mathrm{LE}}$ is the frontal area of the flat-faced portion of the wing. Equations (7) and (8) will be integrated into the AP02 code for Mach numbers 0.85 and below. For Mach numbers between 1.05 and 0.85, linear interpolation is used between the AP02 values for the wing wave drag at $M = 1.05$ and the value computed by Eqs. (7) and (8) at $M = 0.85$. Note that if the wing leading edge is rounded vs being truncated, no appreciable pressure drag occurs on the leading edge at subsonic Mach numbers according to Ref. 14. The current version of the AP02 will give good results for sharp or rounded leading-edge wings, and so no modifications are needed for these wing shapes.

Two-Dimensional Wing Base Pressure Coefficient Improvements

When the accuracy of the wing axial force coefficient for wings that had blunt trailing-edge fins was assessed, it was found the accuracy could be improved on. It was concluded the accuracy problem was attributed to the values of two-dimensional base pressure coefficient at transonic and subsonic Mach numbers. This conclusion was based on flight-test data[15] for a configuration that had large wings with both sharp and truncated trailing edges. As a result of this conclusion, improved two-dimensional base pressure coefficients were derived empirically and are given in Table 3. As seen in Table 3, the AP05 values deviate from the AP02 values for Mach numbers less than 1.3.

Table 3 Improved values of the two-dimensional base pressure coefficient for AP05

	$C_{P_{2\text{-D}}}$	
M_4	AP02	AP05
0.00	0.240	0.430
0.50	0.260	0.430
0.70	0.285	0.430
0.80	0.305	0.450
0.85	0.325	0.480
0.90	0.345	0.520
1.00	0.440	0.610
1.05	0.435	0.580
1.10	0.430	0.550
1.20	0.420	0.450
1.30	0.390	0.390
1.50	0.337	0.337
1.70	0.285	0.285
1.90	0.245	0.245
2.10	0.213	0.213
2.30	0.186	0.186
2.50	0.165	0.165
2.80	0.115	0.115
3.10	0.095	0.095
3.70	0.078	0.078
4.00	0.070	0.070
4.30	0.055	0.055

Truncated Nose Drag Improvements for Mach Numbers Below 1.2

Another area of weakness in the AP02 is transonic and subsonic pressure drag when the body nose has a large truncated portion vs rounded or sharp. The AP02 uses the methods of Wu and Aoyoma[16] or a full potential solution[17] for sharp or blunt bodies in transonic flow in a table lookup fashion. However, neither of these approaches are accurate or even applicable for truncated noses. As a result, a semi-empirical approximation was derived, using data from Ref. 18, to approximate the additional axial force coefficient for $M_\infty < 1.2$ when the nose has a truncated tip. The new method will be briefly summarized here. For details of the new method, the reader is referred to Ref. 11.

To solve the truncated nose tip axial force problem for $M_\infty < 1.2$ of the AP02, an empirical term will be added to the axial force coefficient for $M_\infty < 1.2$. The empirical term is defined based on the experimental data of Ref. 18 minus values of base drag, skin-friction drag, and wave drag for $0.7 < M_\infty < 1.2$ predicted by the AP02. Using this approach to modify the wave drag term for truncated nose tips for $M_\infty < 1.2$, we define

$$\Delta C_{A_W} = C_1(M) C_{P_0}\left(\frac{\mathrm{d}_N}{\mathrm{d}_{\mathrm{ref}}}\right)^2\left(\frac{2\mathrm{d}_N}{\mathrm{d}_{\mathrm{ref}}} - 1\right), \qquad \frac{\mathrm{d}_N}{\mathrm{d}_{\mathrm{ref}}} > 0.5$$

$$\Delta C_{A_W} = 0, \qquad \frac{\mathrm{d}_N}{\mathrm{d}_{\mathrm{ref}}} \le 0.5 \tag{9}$$

where

$$C_1(M) = \begin{Bmatrix} 0.73; & M_\infty \le 0.7 \\ 1.29 - 0.8M_\infty; & 0.7 < M_\infty \le 1.05 \\ 3.45 - 2.88M_\infty; & 1.05 < M_\infty < 1.2 \end{Bmatrix} \tag{10}$$

C_{P_0} of Eq. (9) is defined by Eq. (8) and $\mathrm{d}_N/\mathrm{d}_{\mathrm{ref}}$ is the ratio of the nose truncated tip diameter to the reference diameter. The last term of Eq. (9) was arrived at based on comparison of the AP02 to a configuration that had a 50% truncated nose tip bluntness with a nose length of 0.75 calibers. For the 50% nose tip bluntness, the AP02 predictions agreed reasonably well with experimental data. This leads one to conclude the additional nose pressure drag from truncated nose tips in subsonic and transonic flow comes from large truncated nose tips $\mathrm{d}_N/\mathrm{d}_{\mathrm{ref}} > 0.50$. Unfortunately, Ref. 18 did not have data for configurations other than $\mathrm{d}_N/\mathrm{d}_{\mathrm{ref}} = 1.0$ and 0.5. As a result, a linear interpolation of the ΔC_{A_W} term of Eq. (9) is assumed between the $\mathrm{d}_N/\mathrm{d}_{\mathrm{ref}}$ values of 0.5 and 1.0.

Trim Aerodynamics Output

One of the major applications of the aeroprediction code is to provide trim aerodynamics for inputs to a three-degree-of-freedom (3-DOF) simulation model. Trim aerodynamics are defined at AOA where the pitching moment about the center of gravity is zero. The AP02 incorporates a 3-DOF model with the aerodynamics code, and trim aerodynamics are computed automatically and used as inputs for the trajectory model. However, for those engineers who still want to use the APC to provide trim aerodynamics to their own 3-DOF model, the engineer must perform this task iteratively with the AP02. Typically, a control deflection is chosen and the AOA found iteratively through trial and error that allows zero pitching moment. When several control deflections are assumed at each of several Mach numbers, this process can take about a day for an experienced engineer.

The AP05 provides an option for the user to allow the calculation and output of trim aerodynamics. This option will save considerable time and dollars for those who want to perform this task on many configurations. Typical outputs are trim values of C_A, C_N, C_D, and C_L for various values of control deflection, Mach number, and trim

AOA. A new set of plots are also available in the postprocessor of the AP05 for trim aerodynamics.

Protuberance Aerodynamics Input Option

The AP02 and all prior versions of the APC allow inputs for a rotating band if the weapon is a spin-stabilized projectile. However, many weapons have irregular shapes on the outside of the body, which can contribute slightly to the aerodynamics. Examples of some of these external configuration protuberances include electronic guide wires on missiles from the forward guidance to aft control surfaces, slots located both longitudinally and circumferentially around the body, and screw threadlike grooves used in launching certain projectiles. Some protuberance aerodynamics can be approximately modeled by the APC, but most can not be accurately predicted. As a result of this deficiency in the AP02, the AP05 will allow static aerodynamics to be input for protuberances. These additional inputs for protuberances allow terms for axial- and normal-force and pitching moment coefficients. The change in center of pressure due to protuberances can be calculated directly from the protuberance inputs for pitching moment and normal force. Also note that one can input protuberance terms for axial force coefficient only, with ΔC_{N_α} and ΔC_{M_α} being zero. The protuberance axial force inputs are allowed to vary with Mach numbers but are given at some AOA and assumed to be constant at other AOA. The protuberance aerodynamic inputs for normal-force and pitching moment coefficient are defined in terms of slopes, that is, ΔC_{N_α} and ΔC_{M_α}, which are allowed to vary with Mach number. Since they are linear slopes, they should be expected to give changes in ΔC_N and ΔC_M at low AOA or one can choose to take average changes with AOA. Also, ΔC_A, ΔC_{N_α}, and ΔC_{M_α} can be input at both the $\Phi = 0$ and $\Phi = 45$ deg roll orientation if wings are present. If the configuration is a body alone, only $\Phi = 0$ deg roll is allowed.

User-Defined Boundary-Layer Transition for Body and Wing

The AP02 has four boundary-layer options. These include all laminar flow, wind-tunnel model with or without a boundary-layer trip, and typical flight. For the all laminar flow case, the APC artificially sets a very high transition Reynolds number in the code so that the flow will remain laminar over the wings and body. For the wind-tunnel model with boundary-layer trip, the APC artificially sets a very low value of transition Reynolds number in the code so that the flow is turbulent over the body and lifting surfaces. Typical flight means you want to obtain axial force you would expect for a weapon in flight, not in a wind tunnel. Typical flight assumes a transition Reynolds number of 1×10^6 on the body and 0.5×10^6 on the wings. For the wind-tunnel model with no boundary-layer trip, transition Reynolds numbers of 4×10^6 and 2×10^6 for the body and wings, respectively, are assumed.

Whereas the four boundary-layer transition options discussed cover many options the engineer would like to model, there are some cases that do not fit within the four options given. Some of these include different transition Reynolds number for the wind-tunnel model with no boundary-layer trip option than the ones assumed. In some cases, the body may have a trip and the lifting surfaces do not. Also, a ballistic range model may be somewhere in between the wind-tunnel and free-flight transition Reynolds number, and in some cases, a boundary-layer trip may be effective at some Mach numbers, but at other Mach numbers the flow may relaminarize. As a result of the desire to have more boundary-layer transition alternatives, the AP05 will include a fifth option. The fifth option will allow the user to define individual boundary-layer transition Reynolds numbers for the body and the wings. This new option will allow the user more flexibility in accurately modeling the skin-friction drag component of the axial force, assuming the user knows what the transition Reynolds number is. If the user has axial-force experimental data, but does not know the transition Reynolds number, the user can use the AP05 code in a trial and error mode to select a transition Reynolds number that more closely matches the data. This transition Reynolds number could then be used for other AP05 computations on the same configuration, assuming of course the model size and external smoothness remained the same.

Small Caliber Weapons

At a recent AP02 theory and users course taught at Picatinny Arsenal in New Jersey, it was found that, for small diameter ammunition, the AP02 gave predicted aerodynamics that varied considerably as the diameter decreased below about 12 mm. When the root cause of the problem was examined, it was concluded that not enough decimal places were allowed for the input geometry read statements. The read statements in the original FORTRAN code required all dimensions to be input in feet and areas in square feet. Four digits behind the decimal point were allowed for linear dimensions, and five digits for areas were allowed. For diameters of 12 mm and greater, the input geometry accuracy proved satisfactory to give consistent accuracy on aerodynamics. However, for small caliber ammunition, inconsistent results were obtained. The AP05 solved this problem by increasing the number of digits behind the decimal point for linear dimensions to six places from four and areas to eight from five. The AP05 now gives consistent aerodynamics for diameters as small as 1 mm. It is believed the AP05 can, therefore, be used for all diameter weapons, whereas the AP02 was limited to 12-mm diameter and higher to get consistent results.

Increase in Altitude Limits for Trajectory Models

The AP02 code was limited in altitude to 250,000 ft, which is about where the atmosphere begins to transition from continuum to free molecular flow. Continuum flow equations (such as the Navier–Stokes, Euler, etc.) can be used in altitude up to about 500,000 ft but with a slip boundary condition in the viscous equations vs a no-slip condition. As shown in Chap. 2 of Ref. 17, the aerodynamic forces and moments become very small for altitudes greater than about 250,000 ft and can, therefore, be neglected compared to the vehicle weight for many applications. However, regardless of the size of the aerodynamic forces and moments, there have been applications where the user has desired to generate trajectories that have altitudes greater than 250,000 ft.

Trajectory models have all forces and moments included, including the Earth's gravitational pull, which is also a function of altitude. Hence, even though the aerodynamic forces can be neglected at high altitude for many applications, the weapon still flies in a near vacuum,[19] governed primarily by the force of gravity in the conservation equations of motion. The AP05 code will, therefore, allow the weapon to continue to fly above 250,000 ft, whereas the AP02 will not.

AP02 Errors Corrected for AP05

There were several errors in the AP02 that were corrected and, therefore, will result in more robustness and better accuracy for the AP05 compared to the AP02 for cases where those errors had an impact. The first of these errors had to do with the inconsistency of wave drag when the smoother was on. The total axial-force coefficient was smoothed correctly, but the wave drag term was not corrected to be consistent with the total axial-force coefficient. This inconsistency was corrected for the AP05.

A second problem was found for the roll position of 45 deg, for values of $\alpha + \delta \geq 40$ deg, and for Mach numbers between 2.01 and 2.5. This problem gave erroneous results in the static aerodynamics and has been corrected for the AP05.

A third problem was also uncovered at the roll position of 45 deg at subsonic Mach numbers when α and δ were opposite signs. This problem caused the code to malfunction at certain conditions. Again, this problem was solved and was fixed for the AP05.

A fourth problem fixed was the transonic wing-alone lift generated by airplane DATCOM to incorporate thickness effects. It has been found over the years that the thickness effects derived based on aircraft wings appear to be exaggerated for missile configurations. As a result, the wing-alone thickness effect on normal-force coefficient at transonic speeds was decreased by a factor of four over the airplane DATCOM predictions.

In addition to the aforementioned corrections in the FORTRAN code of the APC, there were several corrections made to the pre- and postprocessor for the code. These corrections involve correcting the dimensions on several of the screens in the ballistic model and aerothermal model.

We typically spend several months in validating a code before releasing it to the public. The AP05 will be treated the same; however, there are sure to be errors we will not catch. We appreciate feed back from users when they find a problem. Sometimes the problem is with user inputs, but other times it may be a code error.

Summary of Aerodynamic Methods

The preceding section of this paper summarized the new methods that will be included in the AP05 that were not available in the AP02. In Ref. 17 the methods used in the AP72 up through the AP98 are summarized. In Ref. 8 the new methods for the AP02 are summarized. In general, all versions of the APC are based on SBT, linear theory, or second-order theory at low AOA and empirical methods at high AOA. The low AOA theoretical methods gives the APC a good foundation to predict aerodynamics for various geometries and for various flight conditions up to AOA of about 10 deg. The empirical methods were developed based on large wind-tunnel component databases, in conjunction with total configuration databases, and allowed the low AOA theoretical methods to be extended to 90-deg AOA. The overall approach of combining the low AOA methods with the wind-tunnel databases to form a semi-empirical APC is described in Ref. 17, Chaps. 3 and 5.

A summary of the theoretical methods that make up the AP05 are shown in Tables 4–7. Table 4 gives the body-alone methods, Table 5 provides the wing and interference methods, Table 6 shows the dynamic derivative methodology, and Table 7 gives the trajectory and trim aerodynamics options for the AP05. In Tables 4–7 the new technology integrated into the AP02 that makes up the AP05 is noted.

Results and Discussion

Example cases will now be shown for many of the new AP05 technologies discussed earlier in this paper.

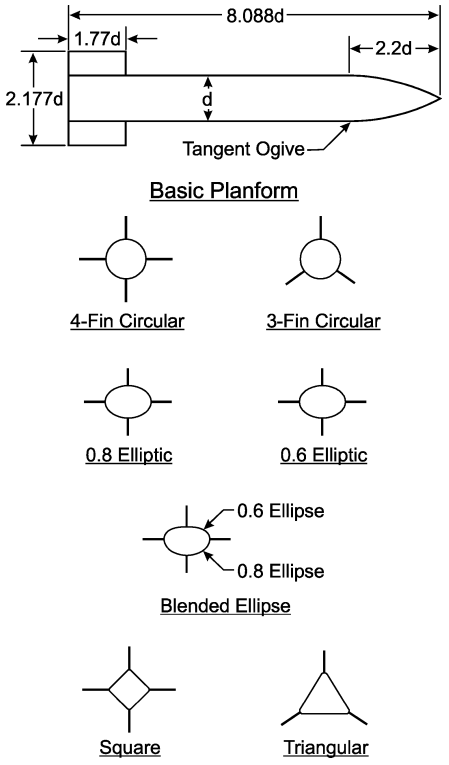

Fig. 3a Model cross section configurations (from Ref. 20).

Multifin Aerodynamics and Truncated Leading-Edge Effects

One example will be shown to illustrate the application of the new three-fin aerodynamics capability to the existing four-, six-, and eight-fin capability of the AP02.

The case considered is the triangular cross-section configuration of Fig. 3a. Figure 3a configurations are taken from Ref. 20, where aeroballistic range tests at the Aeroballistic Range Facility (ARF) were conducted for various circular and noncircular cross section shapes. For the triangular configuration of Fig. 3a, both the AP02 and AP05 can be used to predict aerodynamics because the triangular cross section methodology of the original AP98 assumed three fins. However, the noncircular cross-section methodology developed for the AP98 assumed the three fins were oriented in the horizontal

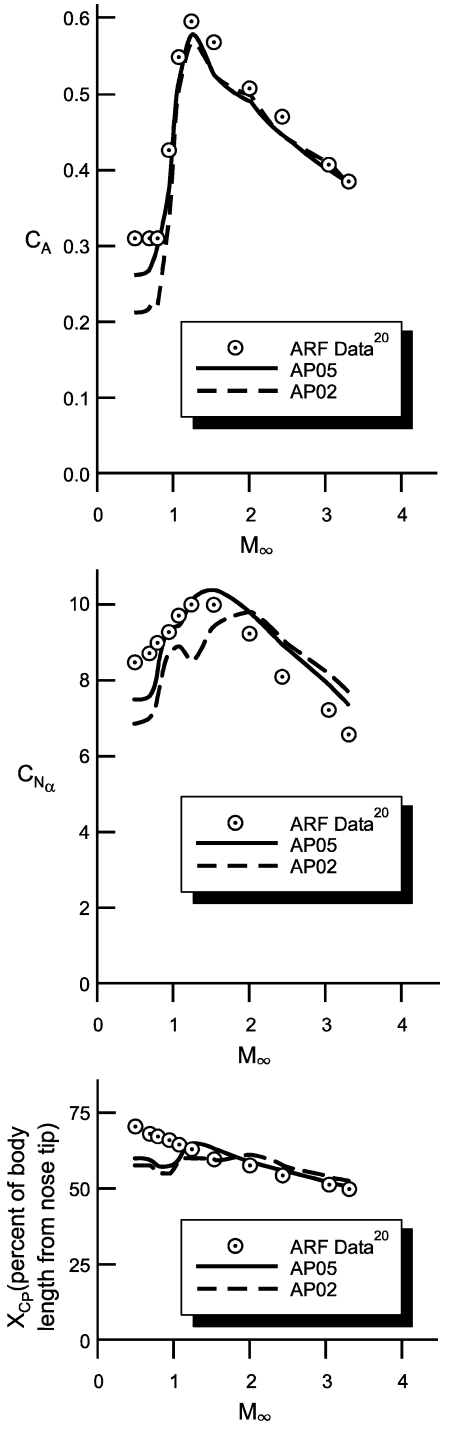

Fig. 3b Comparison of theory and experiment for three-fin triangular shape of Fig. 7a.

Table 4 AP05 methods for body-alone aerodynamics

Component	Subsonic $M_\infty < 0.8$	Transonic $0.8 < M_\infty < 1.2$	Low supersonic $1.2 < M_\infty < 1.8$	Mod/high supersonic $1.8 < M_\infty < 6.0$	Hypersonic $M_\infty > 6.0$
Nose wave drag[a]	Improved empirical[a]	Improved semiempirical based on Euler solutions[a]	Second-order Van Dyke plus MNT	SOSET plus IMNT	SOSET plus IMNT modified for real gases
Boattail or flare wave drag	- - -	Wu and Aoyoma	Second-order Van Dyke	SOSET	SOSET for real gases
Skin-friction drag[a]	Van Driest II with more boundary-layer transition options[a]				
Base drag	Improved empirical method				
Power-off	Emprical				
Power-on	Modified Brazzel method				
Base bleed	Modified Danberg method				
Axial force at α	Empirical method				
Aeroheating information	- - -				SOSET plus IMNT for real gases
Inviscid lift and pitching moment	Empirical	Semiempirical based on Euler solutions	Tsien first-order crossflow	SOSET	SOSET for real gases
Viscous lift and pitching moment	Improved Allen and Perkins crossflow				
Nonaxisymmetric body aero					
Lifting properties	Modified Jorgensen				
Axial force	Modified axisymmetric body				
Nonlinear structural loads available ($\Phi = 0$, 45 deg)	No		Yes		
Protuberance aero input options[a]	Yes				
Accurate small caliber arms aero[a]	Yes				

[a]New technology integrated into AP02 that makes up AP05.

plane vs being oriented at 120 deg apart, as shown in Fig. 3a. To calculate the best answers AP02 or AP05 will provide for this configuration will require two separate computations for the AP02 and one for the AP05. We will consider AP02 computations first. The first AP02 computation is for axial force coefficient where three fins of the correct span (20 mm) is used in the computation process. The second AP02 computation is for lifting properties, where the correct span in the horizontal plane must be used. This value of span is $20\cos^2 30\ \text{deg} = 15$ mm. The reason for the $\cos^2 30$ deg is that the normal force of a fin is always perpendicular to the fin and the fin area in the 30-deg plane projected to the horizontal plane gives the second cos 30 deg. This example illustrates how a configuration that does not fit exactly into the methodology on which the AP02 was developed can still be considered by appropriate design changes and appropriate knowledge of aerodynamics theory. On the other hand, the three-fin methodology of the AP05 accounts for the $(\cos 30\ \text{deg})^2$ term, as shown in Fig. 1. Thus, the three-fin triangular configuration aerodynamics can be computed with one calculation using the true value of wing span of 20 mm.

The results of the two separate calculations for axial and lifting properties for the AP02 and AP05 compared to the ARF data is shown in Fig. 3b. Note that the AP05 gives slightly improved results for the C_A, C_{N_α}, and X_{CP}/d, over the AP02 compared to ballistic range data. Agreement of the AP05 theory and experiment is quite good for C_A and fair to good for C_{N_α} and $X_{\text{CP}}/d_{\text{ref}}$. The improvement in C_A is due to both the truncated leading- and trailing-edge improvements in axial force discussed earlier in the paper.

Wing Trailing-Edge Aerodynamics

This section of the paper will consider an example to validate the new methodology to incorporate trailing-edge bluntness effects on normal-force and axial-force coefficient.

The configuration is a typical guided projectile concept with 8 tail fins for stability. It is 12.17 calibers in length with a low drag nose and a boattail (Fig. 4a). The unpublished wind-tunnel test data (provided to Aeroprediction, Inc., by Seth Renaldi of the U.S. Naval Surface Weapons Center, Dahlgren Division) was for fins with a single wedge, except at $M_\infty = 3.5$, where both single and double wedge fins were tested. The fin cross-sectional shapes are shown in Fig. 4a. Figure 4b shows a comparison of the AP05 predictions for both the single-wedge (SW) and double-wedge (DW) cases to the SW experimental data. The DW axial-force experimental data at $M = 3.5$ was approximately the same as the SW value. Note the improved predictions of the AP05 compared to experiment and the AP02 for $M_\infty < 1.3$. In general, good agreement with experiment is seen, particularly with the AP05.

Figures 4c and 4d show a comparison of the theory to experiment for both the normal-force coefficient derivative and the center of pressure. The values shown in Figs. 4c and 4d were derived based on experimental data of 2-deg AOA, and the AP02 and AP05 calculations were performed at 2-deg AOA also. Note in Figs. 4 that the AP02 gives the same values for C_{N_α} and X_{CP} for the SW and DW fins, whereas the AP05 shows improvements in predictions for both the SW and DW. The DW improvements come from adding an aspect ratio of 4 in Table 2, whereas the AP02 uses aspect ratio 2 data for all aspect ratios 2.0 and greater. The SW improvements in Figs. 4c and 4d come from both the Table 2 extension as well as the new methods of Eqs. (2) and (7). In general, the AP05 shows improvement compared to experiment over the AP02. The AP05 shows good agreement to experiment for C_{N_α}. The center of pressure is predicted too far forward by about a half a caliber at transonic speeds. Of particular importance is the comparison of the AP05 SW and DW data to experiment at Mach 3.5. Whereas the absolute value of the theory is off slightly for both C_{N_α} and X_{CP}, the magnitude of the experimental difference between the SW and DW is predicted quite

Table 5 AP05 methods for wing-alone and interference aerodynamics

Component	Subsonic $M_\infty < 0.8$	Transonic $0.8 < M_\infty < 1.2$	Low supersonic $1.2 < M_\infty < 1.8$	Mod/high supersonic $1.8 < M_\infty < 6.0$	Hypersonic $M_\infty > 6.0$
Wave drag[a]	Semi-empirical[a]	Improved semi-empirical[a]	Linear theory plus MNT	Shock Expansion (SE) plus MNT along strips	SE plus MNT for real gases along strips
Skin-friction drag[a]	Van Driest II with more boundary-layer transition options[a]				
Trailing edge separation drag	Improved empirical[a]				
Body base pressure caused by tail fins	Empirical				
Inviscid lift and pitching moment	Lifting surface theory	Empirical	3DTWT	3DTWT	3DTWT
Linear			Linear[a]		
Nonlinear			Empirical[a]		
Impact of trailing Edge bluntness			Semi-empirical[a]		
Wing–body, body–wing interference ($\Phi = 0$, 45 deg)					
Linear	Slender body theory or linear theory modified for short afterbodies				
Nonlinear	Improved empirical				
Wing–body interference due to δ ($\Phi = 0$, 45 deg)					
Linear	Slender body theory				
Nonlinear	Improved empirical				
Wing–tail interference ($\Phi = 0$, 45 deg)	Line vortex theory with modifications for $K_{W(B)}$ term and nonlinearities				
Aeroheating	None present		SE plus MNT		SE plus MNT real gases
Nonaxisymmetric body aero ($\Phi = 0$, 45 deg)	Improved Nelson method				
Nonlinear st. loads available ($\Phi = 0$, 45 deg)	No		Yes		
2, 3, 4, 6, 8 fin aero[a]					
Linear[a]	Slender body theory[a]				
Nonlinear[a]	Semi-empirical (CFD + data)[a]				
Trailing-edge flaps on tails	Semi-empirical (seek tail deflection for equal normal force)				

[a]New technology in AP05.

Table 6 AP05 methods for dynamic deratives

Component	Subsonic $M_\infty < 0.8$	Transonic $0.8 < M_\infty < 1.2$	Low supersonic $1.2 < M_\infty < 1.8$	Mod/high supersonic $1.8 < M_\infty < 6.0$	Hypersonic $M_\infty > 6.0$
Body alone					
No flare			Empirical		
With flare			Semi-empirical		
Wing and interference roll damping moment	Lifting surface theory	Empirical		Linear thin wing theory	
Wing magnus moment			Assumed zero		
Wing and interference pitch damping moment	Lifting surface theory	Empirical		Linear thin wing theory	

Table 7 Trajectory and trim aerodynamics capability within APC

Simulation mode	AP72–AP98	AP02	AP05
Particle	None		
Ballistic		Yes	Yes
3 DOF	None	Yes	Yes
Trim aero outputs[a]	None	None	Yes[a]

[a]New technology for AP05.

well. Unfortunately, experimental data for the DW are unavailable for Mach numbers other than 3.5.

Small Caliber Weapon Aerodynamics

One of the problems with the AP02 and all prior versions of the APC is its accuracy when applied to small caliber weapons. Small caliber is here defined as about 12 mm or less. The problem arose as a result of the APC being developed primarily for medium and large caliber weapons (20 mm and larger) and not allowing enough

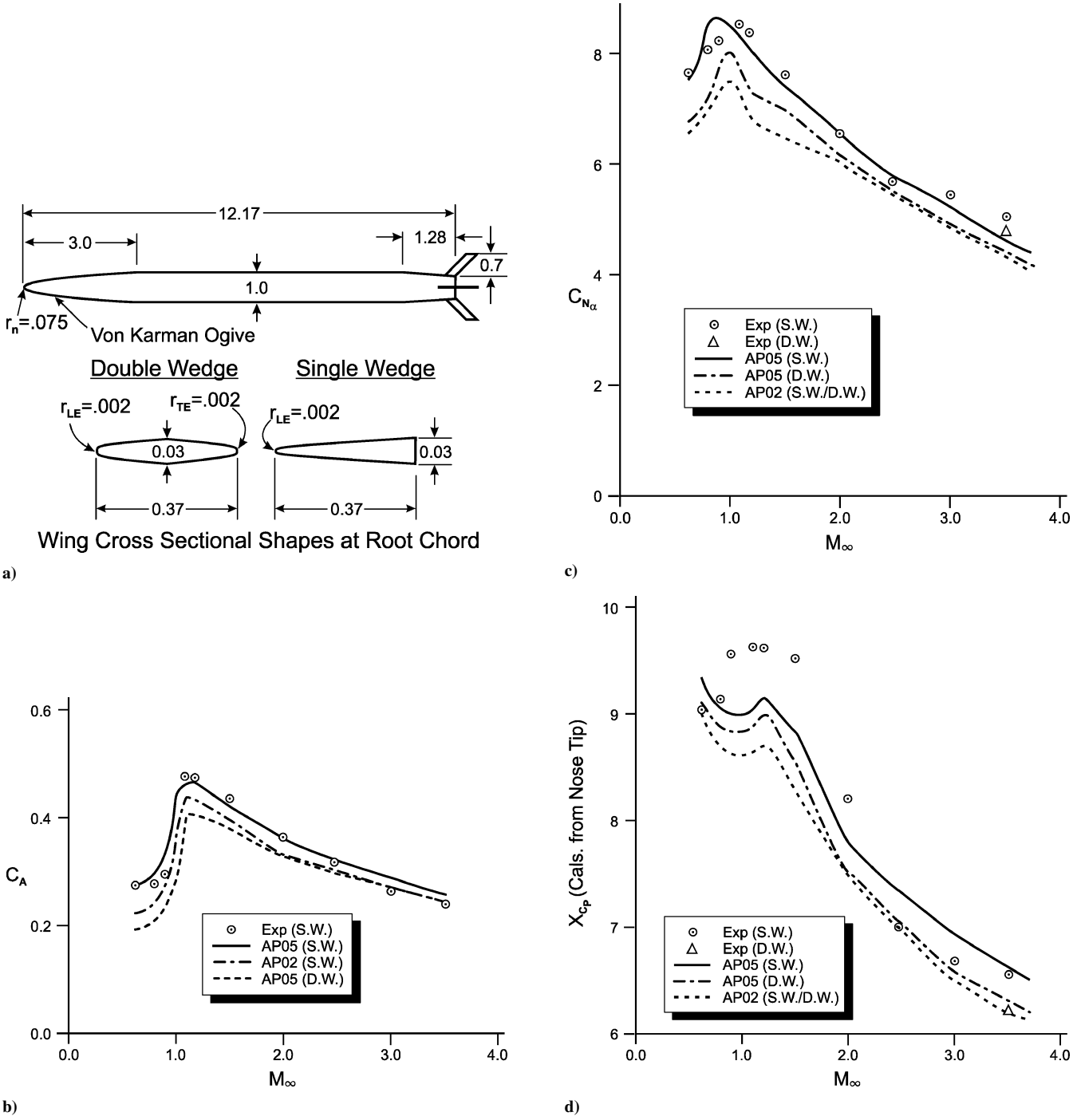

Fig. 4 Configuration of eight-fin guided projectile: a) concept (dimensions in calibers), b) axial force coefficient vs Mach number, c) normal force coefficient derivative, and d) center of pressure.

decimal places for geometry inputs. The AP05 increases the number of decimal places for geometry inputs so that consistent accuracies can be maintained down to at least 1 mm in diameter. The 1-mm diameter is envisioned to be the smallest diameter for practical use.

A practical small diameter case to consider is the Remington 223 round. E. Vazquez of the Picatinny Arsenal in New Jersey provided the external shape and some ballistic range data for the 223 round. Remington places the trajectory information on the back of a box of their shells, which are sold to the public. Unfortunately, the round provided by Vazquez was 55 grains, and the Remington shells that range information was available on were 50 grains. Hence, because the external shape of the rounds is the same, we can compare the AP05 aerodynamics to the range data. Then we can use the external aerodynamics along with the weight and other information from the box of Remington 223 shells to compare the predicted AP05 trajectory. Figure 5a shows the external design of the 223 round, with the dimensions in calibers (1 caliber = 0.223 in.) Figure 5b then gives the axial force information of the 223 projectile range data and the AP05. Results for the AP05 are given at three AOA based on the flight data provided to API as having angle of yaw between about 2 and 11 deg. As seen in Fig. 5, the bullet apparently has its maximum yaw out of the barrel, which is fairly typical for most ammunition. When the Mach number has decreased to 1.6, the angle of yaw appears to have decreased to about 5 deg, and when the bullet has decreased in Mach number to 1.25, the angle of yaw is close to zero.

For the ballistic trajectory simulation, one can not vary the AP05 AOA calculations because the ballistic model assumes a zero AOA.

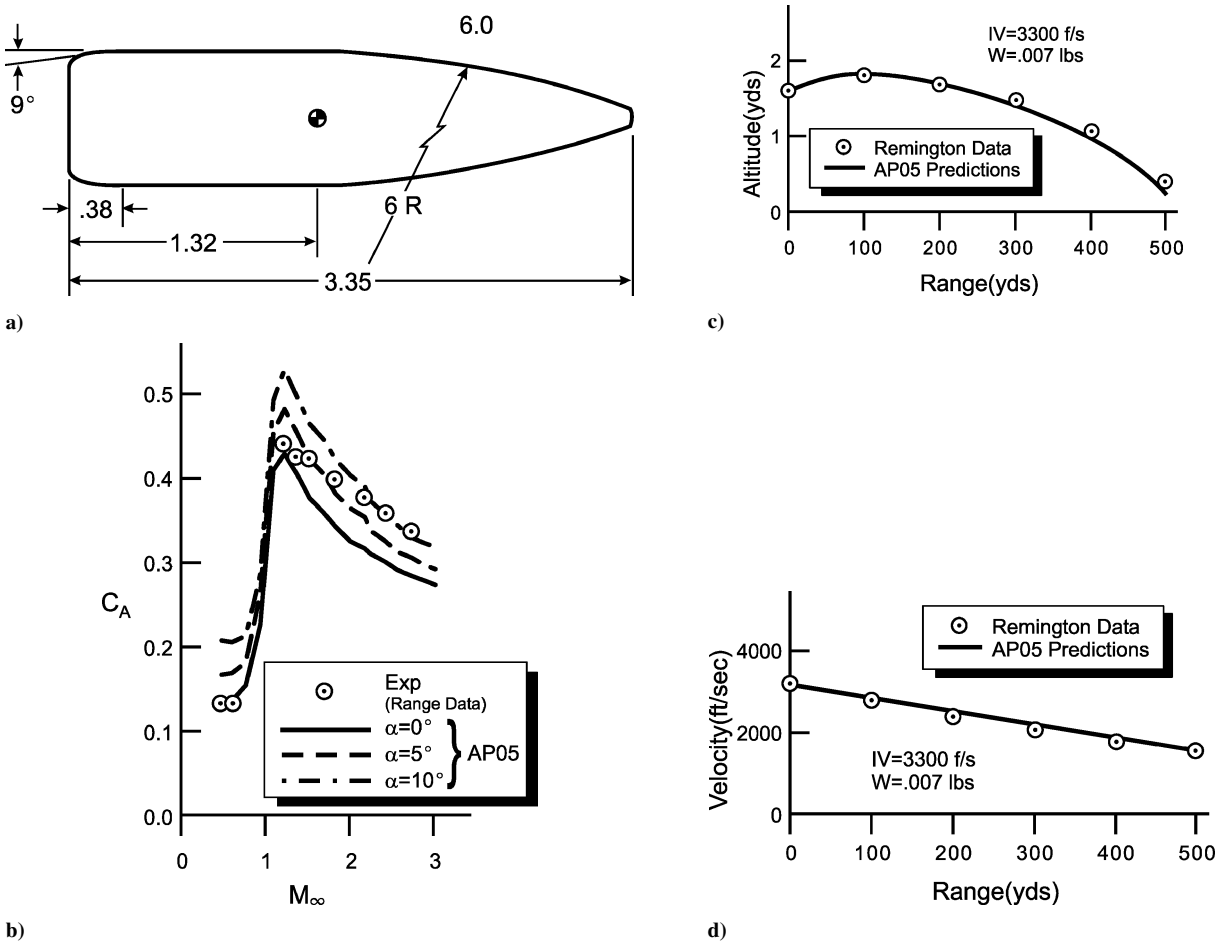

Fig. 5 Remington 223 projectile: a) configuration (all dimensions in calibers), b) comparison of axial force between AP05 and range data, c) comparison of altitude vs range data and AP05, and d) comparison of velocity vs range data and AP05.

However, the ballistic model has a form factor that allows one to account for the variation in drag due to AOA variation. A form factor of 1.037 does a good job in matching the Remington trajectory with the AP05 trajectory. This says, on average, the C_D of the actual trajectory is about 3.7% higher than the zero AOA axial force of Fig. 5b.

Figures 5c and 5d show a comparison of the actual trajectory given by Remington for the 223 round to that predicted by the AP05. The round was sighted in by Remington at 200 yd, which means the gun was elevated slightly so the bullet would hit the bullseye at 200 yd.

The actual data used by Remington is as follows: initial velocity (IV) = 3300 ft/s, crosswind = 10 mph, sights 1.5 in. above bore, and weight = 50 grains = 0.007 lb.

The inputs for the AP05 trajectory model are as follows: IV = 3300 ft/s, crosswind = 10 mph, elevation = 3.5 min, form factor = 1.037, AOA = 0 deg, height at launch = 5 ft, and weight = 0.007 lb.

Figure 5c gives the altitude vs range comparison, and Fig. 5d shows a comparison of the velocity vs range. As seen in both Figs. 5c and 5d, the AP05 predicts the trajectory very well. However, as already noted, a form factor of 1.037 was needed to account for the AOA drag in the actual trajectory with the zero AOA predictions using the AP05 code.

Protuberance Aerodynamic Inputs Example

The only protuberance option in the AP02 is for a rotating band on a spin-stabilized projectile. No option exists for any other weapon. Many weapons have external protuberances that cause a small, yet significant change in the aerodynamics. Some of these protuberances include wiring tunnels, waveguides, rollerons, mounting lugs, slots, etc. It is very difficult to automate an aerodynamic computation process for protuberances because the aerodynamics can be a function of AOA, Mach number, and location on the body as a function of roll orientation. The present approach of handling external configuration perturbations on configuration aerodynamics is to compute the perturbation aerodynamics by hand, compute the smooth configuration aerodynamics with the AP02, and then manually add the ΔC_A, ΔC_N, and ΔC_M to the AP02 numbers off-line.

The AP05 will reduce the labor involved in the preceding process by giving the user a protuberance input option that allows variations in M_∞ and Φ (roll positions of 0 and 45 deg only). The AOA variation in ΔC_N and ΔC_M will be partially accommodated by including ΔC_{N_α} and ΔC_{M_α}. Hence, one could take the variation at low AOA in ΔC_N and ΔC_M or some variation at larger AOA. ΔC_A is not allowed to vary with AOA. The user will still have to determine the protuberance aerodynamics either manually or from experimental data, but the addition of these aerodynamics to the AP05 can be done as part of the inputs for a given case. The advantage of this approach is that the AP05 outputs (tables, plots, and component listing) will now include all of the totals. The protuberance inputs will always be added to the body terms.

The example shown in Fig. 6a is a wind tunnel model of a version of the Seasparrow missile. This missile configuration was tested[21] at $M_\infty = 2.3$ and 4.6 for AOA 45–90 deg and roll angles of 0 and 45 deg. Note in Fig. 6a the wiring tunnels located at roll position of 135 and 315 deg when the fins are at roll position of 0 deg (fins in plus fin arrangement) and the waveguide located at roll position of 225 deg. Figure 6b shows the geometry details of the waveguide and wiring tunnels.

Reference 22 also has wind tunnel data for a smooth model of nearly the same configuration. The only difference is that the Ref. 22 model had a small boattail, whereas the Ref. 21 model (Fig. 6a) had

Table 8 Perturbations in static aerodynamics from external protuberances on Seasparrowlike missile ($\Phi = 0$ deg)

	Experimental estimates			Analytical estimates			Smoothed values		
α, deg	ΔC_A	ΔC_N	ΔC_M	ΔC_A	ΔC_N	ΔC_M	ΔC_A	ΔC_N	ΔC_M
				$M_\infty = 4.6$					
0	N/A	0	0	0.013	0	0	0.013	0	0
5	N/A	0	−1.2	0.013	0.01	−0.01	0.013	0.01	−0.01
10	N/A	0	−0.9	0.013	0.03	−0.02	0.013	0.03	−0.1
15	N/A	0	−0.3	0.013	0.07	−0.04	0.013	0.07	−0.2
20	N/A	0.3	−1.5	0.013	0.11	−0.07	0.013	0.2	−0.5
25	N/A	0.4	−1.3	0.013	0.16	−0.10	0.013	0.4	−0.7
30	N/A	0.9	−1.3	0.013	0.22	−0.14	0.013	0.6	−1.0
35	N/A	1.0	−1.0	0.013	0.29	−0.18	0.013	0.9	−1.3
40	N/A	1.2	−3.7	0.013	0.35	−0.22	0.013	1.2	−1.8
				$M_\infty = 2.3$					
0	N/A	0	0	0.019	0	0	0.019	0	0
5	N/A	0.4	−1.0	0.019	0.01	−0.01	0.019	0.1	−0.5
10	N/A	0.4	−1.5	0.019	0.03	−0.02	0.019	0.2	−1.0
15	N/A	0.4	−2.9	0.019	0.07	−0.04	0.019	0.3	−1.5
20	N/A	0.4	−3.0	0.019	0.11	−0.07	0.019	0.4	−2.0
25	N/A	0.8	−2.5	0.019	0.16	−0.10	0.019	0.6	−2.4
30	N/A	0.9	−2.8	0.019	0.22	−0.14	0.019	0.8	−2.8
35	N/A	1.3	−3.4	0.019	0.29	−0.18	0.019	1.0	−3.2
40	N/A	1.2	−3.6	0.019	0.35	−0.22	0.019	1.2	−3.6

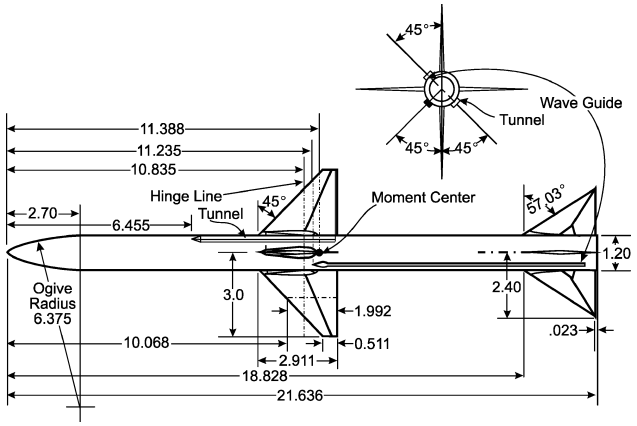

Fig. 6a Configuration with diamond airfoil sections (from Ref. 21) (dimensions are in inches unless otherwise noted).

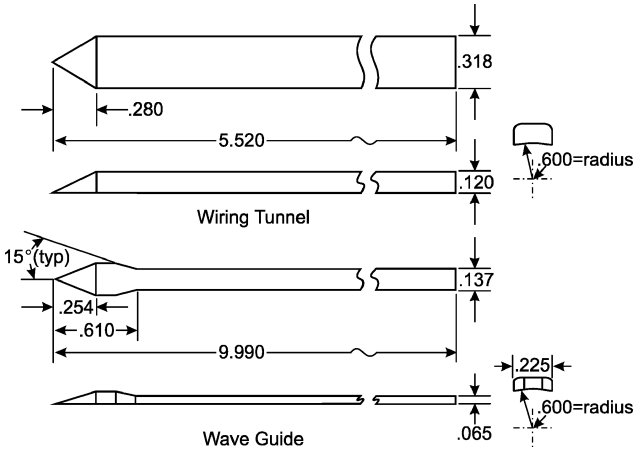

Fig. 6b Details of wiring tunnels and waveguide.

no boattail. In executing the AP05 at $M_\infty = 2.3$ and 4.6, it was found the boattail had a very small impact on C_N ($\leq |0.1|$) and C_M ($\leq |0.12|$) . Unfortunately, the Ref. 21 data only listed C_N and C_M and so no ΔC_A data can be determined from subtracting the Ref. 21 data from the Ref. 22 data. However, ΔC_{N_α} and ΔC_{M_α} can be determined by subtracting the two data sets. Unfortunately, Refs. 21 and 22 data reports only had graphs, not exact numbers from wind-tunnel tests. This means that additional errors are generated as a result of estimating aerodynamics from small figures using two different wind-tunnel tests and two slightly different models.

A second approach to calculate ΔC_{N_α}, ΔC_{M_α}, and ΔC_A is analytically by hand. The hand calculation approach can be used to supplement wind-tunnel data or to replace wind-tunnel data. Also in the case of the Refs. 21 and 22 data, analytical estimates can help smooth out errors encountered by estimating the perturbation quantities from small charts of wind-tunnel data.

To estimate ΔC_A analytically, the shape of the nose contour of the waveguide and wiring tunnels (Fig. 6b) were considered in conjunction with Ref. 23 to estimate the pressure coefficients and then wave drag. No additional axial force calculations were considered for skin friction and base drag. We have also found Ref. 14 quite useful in helping define ΔC_A for various odd-shaped protuberances. To estimate ΔC_{N_α} and ΔC_{M_α}, the waveguide (WG) and wiring tunnels (WTs) were considered to be low aspect ratio wings so that the linear term of normal force and pitching moment was estimated by SBT and the nonlinear term by viscous crossflow theory, that is, for $\Phi = 0$,

$$(\Delta C_N)_{\mathrm{WG}} = \left(\pi AR_{\mathrm{WG}}\alpha/2 + \eta C_{d_c}\sin^2\alpha\right)(A_P/A_{\mathrm{ref}})\cos^2 45 \tag{11a}$$

$$(\Delta C_N)_{\mathrm{WT}} = \left(\pi AR_{\mathrm{WT}}\alpha/2 + \eta\, C_{d_c}\sin^2\alpha\right)(2A_P/A_{\mathrm{ref}})\cos^2 45 \tag{11b}$$

ΔC_{N_α} can be found by taking the derivative with respect to AOA of Eqs. (11a) and (11b) and then adding the two together. Note that AOA appears in both terms of Eqs. (11a) and (11b). Thus,

$$\Delta C_{N_\alpha} = \left(\pi AR_{\mathrm{WG}}/2 + 2\eta C_{d_c}\sin\alpha\right)[(A_P)_{\mathrm{WG}}/2A_{\mathrm{ref}}] + \left[\pi(AR)_{\mathrm{WT}}/2 + 2\eta C_{d_c}\sin\alpha\right][(A_P)_{\mathrm{WT}}/2A_{\mathrm{ref}}] \tag{11c}$$

To compute pitching moment, it was assumed the center of pressure of both the WG and the WTs were at their midchord points. If we wanted to calculate ΔC_A, ΔC_{N_α}, and ΔC_{M_α} at roll of 45 deg, the $\cos^2$ 45 deg in Eqs. (22) becomes $\cos^2 0 = 1$ because both the WG and WTs are at roll position of 0 deg. ΔC_A would remain the same for both roll of 0 and 45 deg.

Tables 8 and 9 give the ΔC_A, ΔC_N, and ΔC_M values approximated from experimental data, analytical calculations, and the final smoothed values that were used for ΔC_{N_α} inputs into the AP05 code. Several points are worthy of note in Tables 8 and 9. First, the experimental values of ΔC_N and ΔC_M are not smooth, showing the difficulty of picking off points from charts accurately.

Table 9 Perturbations in static aerodynamics from external protuberances on Seasparrowlike missile ($\Phi = 45$ deg)

	Experimental estimates			Analytical estimates			Smoothed values		
α, deg	ΔC_A	ΔC_N	ΔC_M	ΔC_A	ΔC_N	ΔC_M	ΔC_A	ΔC_N	ΔC_M
				$M_\infty = 4.6$					
0	N/A	0	0	0.013	0	0	0.013	0	0
5	N/A	0.55	−0.3	0.013	0.02	−0.02	0.013	0.02	−0.03
10	N/A	−0.12	−0.05	0.013	0.06	−0.04	0.013	0.06	−0.05
15	N/A	−0.5	−0.2	0.013	0.14	−0.08	0.013	0.14	−0.10
20	N/A	0.2	−0.3	0.013	0.22	−0.14	0.013	0.20	−0.15
25	N/A	0.7	−0.1	0.013	0.32	−0.20	0.013	0.50	−0.2
30	N/A	1.7	−0.3	0.013	0.44	−0.28	0.013	0.80	−0.3
35	N/A	1.2	−1.25	0.013	0.58	−0.36	0.013	1.10	−1.3
40	N/A	1.3	−2.8	0.013	0.70	−0.44	0.013	1.30	−2.0
				$M_\infty = 2.3$					
0	N/A	0	0	0.019	0	0	0.019	0	0
5	N/A	0.1	0	0.019	0.02	−0.02	0.019	0.05	−0.02
10	N/A	0.1	+0.9	0.019	0.06	−0.04	0.019	0.10	−0.2
15	N/A	0.7	0	0.019	0.14	−0.08	0.019	0.3	−0.3
20	N/A	0.8	−0.9	0.019	0.22	−0.14	0.019	0.5	−0.5
25	N/A	1.4	−1.2	0.019	0.32	−0.20	0.019	0.8	−0.7
30	N/A	1.4	−0.25	0.019	0.44	−0.28	0.019	1.0	−1.0
35	N/A	2.0	−3.1	0.019	0.58	−0.36	0.019	1.3	−1.8
40	N/A	2.3	−3.4	0.019	0.70	−0.44	0.019	1.5	−2.6

Second, the experimental values of ΔC_N and ΔC_M tend to be higher than the analytical values in many cases. Third, the ΔC_N and ΔC_M values at $\Phi = 45$ deg are not twice those at roll $\Phi = 0$ deg, as was expected based on rough analytical calculations. Therefore, there are some interaction effects within the supersonic flowfield not accounted for by the simple analytical approximation. Nevertheless, it is believed the smoothed values of ΔC_N and ΔC_M are better estimates of the true value of ΔC_N and ΔC_M than either the analytical or experimental estimates by themselves.

Because the AP05 perturbation inputs only allows ΔC_A, ΔC_{N_α}, and ΔC_{M_α} as a function of Mach number and roll angle, values of ΔC_{N_α} and ΔC_{M_α} will be computed for an AOA of 30 deg using Tables 8 and 9. This means the ΔC_N and ΔC_M will be slightly high for lower AOA and slightly low for higher AOA. If the user desired to model only small AOA, lower values of AOA would be used.

Figures 7a and 7b shows a comparison of the AP05 predictions (with the Table 8 values for ΔC_{N_α} and ΔC_{M_α} automatically included) for C_N and C_M at $M_\infty = 2.3$ and 4.6 to experimental data for the configuration of Fig. 6 at roll position of $\Phi = 0$ deg.

Figures 7c and 7d give the complementary $\Phi = 45$ deg comparisons of experiment and AP05 predictions for the Fig. 6 configuration. As seen in the Figs. 7a–7d, the AP05 predictions compared to experiment are mostly quite good. Also, note that the ΔC_{N_α} and ΔC_{M_α} additions derived from Tables 8 and 9 improves the AP05 predictions to experiment for most conditions. An exception to the good accuracy of the AP05 is for the pitching moment at $M_\infty = 4.6$ and for $\alpha = 35$ deg, where the experiment shows a marked decrease in static stability compared to predictions. However, even for the worst-case condition C_M comparisons, which is $M_\infty = 4.6$, $\alpha = 40$ deg, and $\Phi = 0$ deg, the AP05 gives a center of pressure error of only 3.4% of the body length. The single point error of 3.4% is below the quoted average accuracy error of less than 4% of the body length for the AP05. Averages should contain several data points over an AOA and Mach number range. Also, the average error on C_N of 5% is well below the quoted average error of less than 10%. The worst-error comparisons on C_N are at lower AOA for $M_\infty = 4.6$ and $\Phi = 45$ deg.

User-Defined Boundary-Layer Transition Example

The discussion of the four boundary-layer transition options for the AP02 along with the fifth user-defined option that will be a part of the AP05 was given earlier as part of the AP05 new capability. The example chosen to illustrate the utility of this fifth option is the ARF database for noncircular cross section configurations shown in Fig. 3a with data given in Ref. 20. This set of configurations is chosen for two reasons. First, a ballistic range model typically would be expected to have a boundary-layer transition Reynolds number somewhere between the alternatives of typical flight configuration (which has a transition Reynolds number on the body of 1×10^6 and on the wings of 0.5×10^6) and the wind tunnel model with no boundary-layer trip option (which has transition Reynolds numbers on the body and wings of 4×10^6 and 2×10^6, respectively). Many ballistic range models, while free flight, are typically machined to be very smooth, similar to wind-tunnel models. Thus, their transition Reynolds numbers can lie between two options available in the AP02.

Second, the fin leading edges of the models in Fig. 3a are 100% truncated. The truncated leading edge implies a turbulent boundary layer over the entire fin. Thus, we will assume boundary-layer transition values as follows: body 4×10^6 and wings 2.5×10^5.

AP05 calculations of axial force will be compared to ballistic range data and the AP02 options available of typical flight and wind-tunnel model with no boundary-layer trip. The configuration of Fig. 3a selected is the four-fin circular case. Figure 8 shows the results of the three boundary-layer calculations, and whereas all three boundary layer options do a pretty good job of predicting the aerodynamics, the user-defined alternative gives slightly better results than the other two alternatives of Fig. 8. One could choose any number of boundary-layer transition options to try to optimize the results of Fig. 8 if desired.

Truncated Nose Aerodynamics

A single example will be chosen to illustrate the improved accuracy of the AP05 compared to the AP02 for truncated nose configurations for $M_\infty < 1.2$. The case and experimental data are taken primarily from Ref. 24, with some supersonic data for the 100% truncated nose from Ref. 14.

The configuration considered for the truncated nose aerodynamics is a flat-faced cylinder with tails. Figure 9a shows the configuration and Figs. 9b–9e present comparisons of C_A and C_N from the AP02 and AP05 to data at Mach numbers of 0.6, 1.0, 1.2, and 1.5, respectively. Figures 9b–9e show the improved axial-force prediction capability of the AP05 over the AP02 for configurations that have large truncated nose tips. Normal-force prediction accuracy of the AP02 and AP05 are both about the same, and both give fair to good predictions for all Mach numbers.

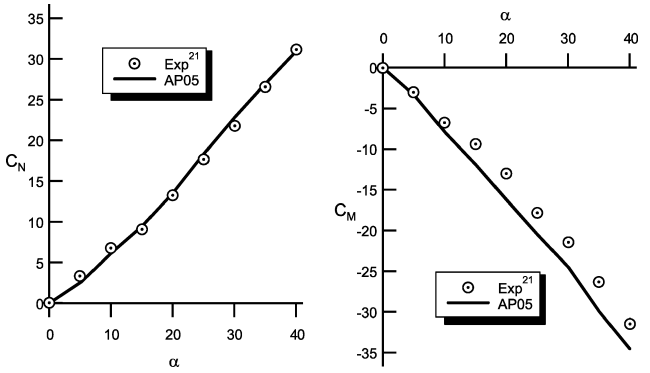

a) $M_\infty = 2.3$, $\Phi = 0$ deg

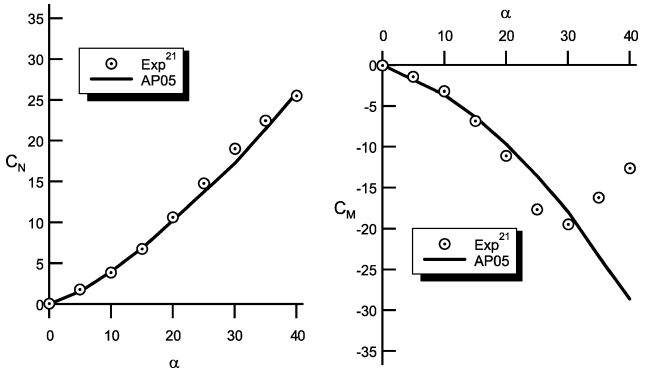

b) $M_\infty = 4.6$, $\Phi = 0$ deg

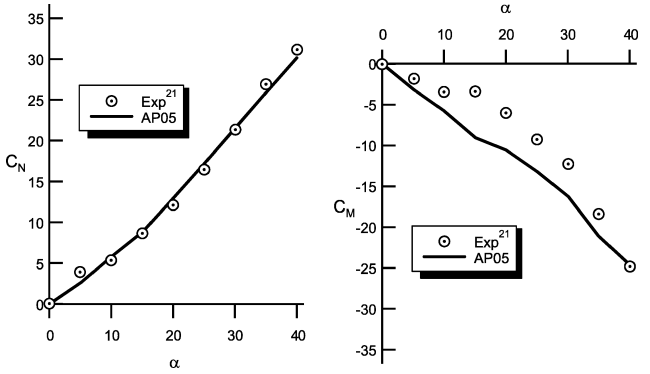

c) $M_\infty = 2.3$, $\Phi = 45$ deg

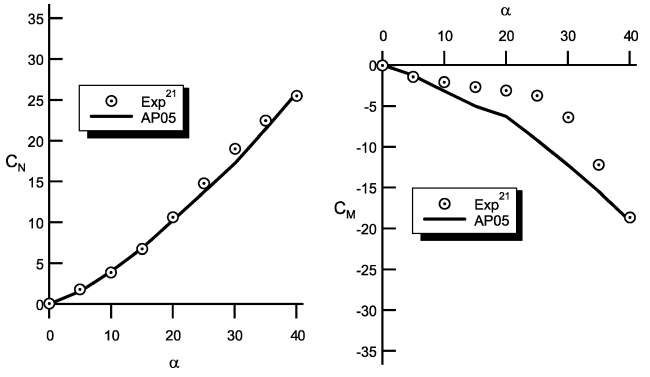

d) $M_\infty = 4.6$, $\Phi = 45$ deg

Fig. 7 Comparison of AP05 predictions to experiment for configuration of Fig. 6a.

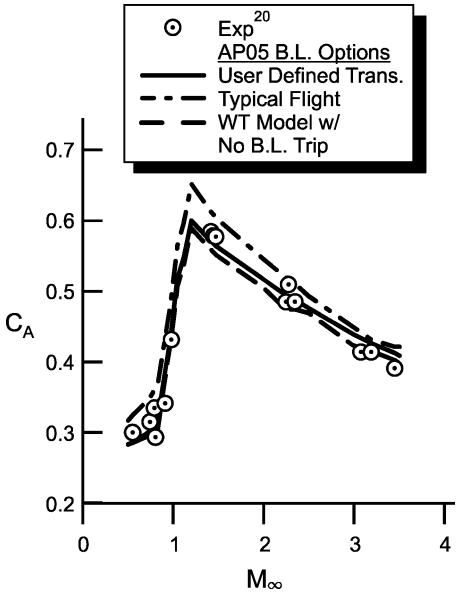

Fig. 8 Comparison of 3 boundary layer transition options in AP05 to ARF range data for 4-fin circular body case.

To summarize the AP05 predictions of aerodynamics on large truncated nose tip configurations, it can be said that significant improvements in accuracy of axial-force coefficients is seen for Mach numbers below 1.2. Normal-force predictions of the AP02 and AP05 are similar and give fair to good agreement with experiment, except for large truncated nose tips in the low supersonic Mach range. At low supersonic Mach numbers of about 1.2, the hybrid theory of Van Dyke tends to underpredict the body-alone normal force compared to experiment, and this underprediction is made worse for large truncated nose tips.

Trim Aerodynamics

One example will be chosen to illustrate the new trim aerodynamics capability that will be available in the AP05. The configuration chosen is a wing-control, wing–body–tail configuration shown in Fig. 10 and the wind-tunnel model details and aerodynamics are given in Ref. 22.

The configuration has a length of about 18 calibers with a tangent ogive nose 2.25 calibers in length. It has wings and tails of fairly high aspect ratios of 2.8 and 2.6, respectively. Data were taken at Mach numbers of 1.5–4.63 for AOA to 40 deg and control deflections of 0 and 10 deg (at M of 1.5 and 2.0) and 0–20 deg (at M of 2.35–4.63). The data were taken at a Reynolds number of 2.5×10^6/ft, and boundary layer trips were also used. The model had a hollow base, and base axial force measurements were given separately in Ref. 22. These results were added to the forebody axial-force measurements to compare with the AP05 predictions to provide some confidence that trim aerodynamics are reasonable.

Figure 11a shows δ_{trim} vs α_{trim} for Mach numbers of 1.5, 2.87, and 4.6 and at $M = 0$ deg. An upper limit of 20 deg on control deflection was used for trim computations. As seen in Fig. 11a, at $M = 4.6$, an AOA of just over 4 deg is the maximum trim possible for the center of gravity location of Fig. 10. For $M = 2.87$, trim AOA approaching 9 deg are achievable, and for $M = 1.5$, even higher trim AOA are possible.

Figures 11b and 11c show the trim values of axial- and normal-force coefficients as functions of trim AOA and for the Mach numbers of 1.5, 2.87, and 4.6 at $\Phi = 0$ deg roll. If one were interested in available maneuver capability at a given trim AOA, the values of $C_{N_{\text{TRIM}}}$ in Fig. 11c could be used in conjunction with the local dynamic pressure and weight of the vehicle to compute maneuverability. The important point is that Figs. 11 were generated in a matter of minutes vs hours or days with the AP02.

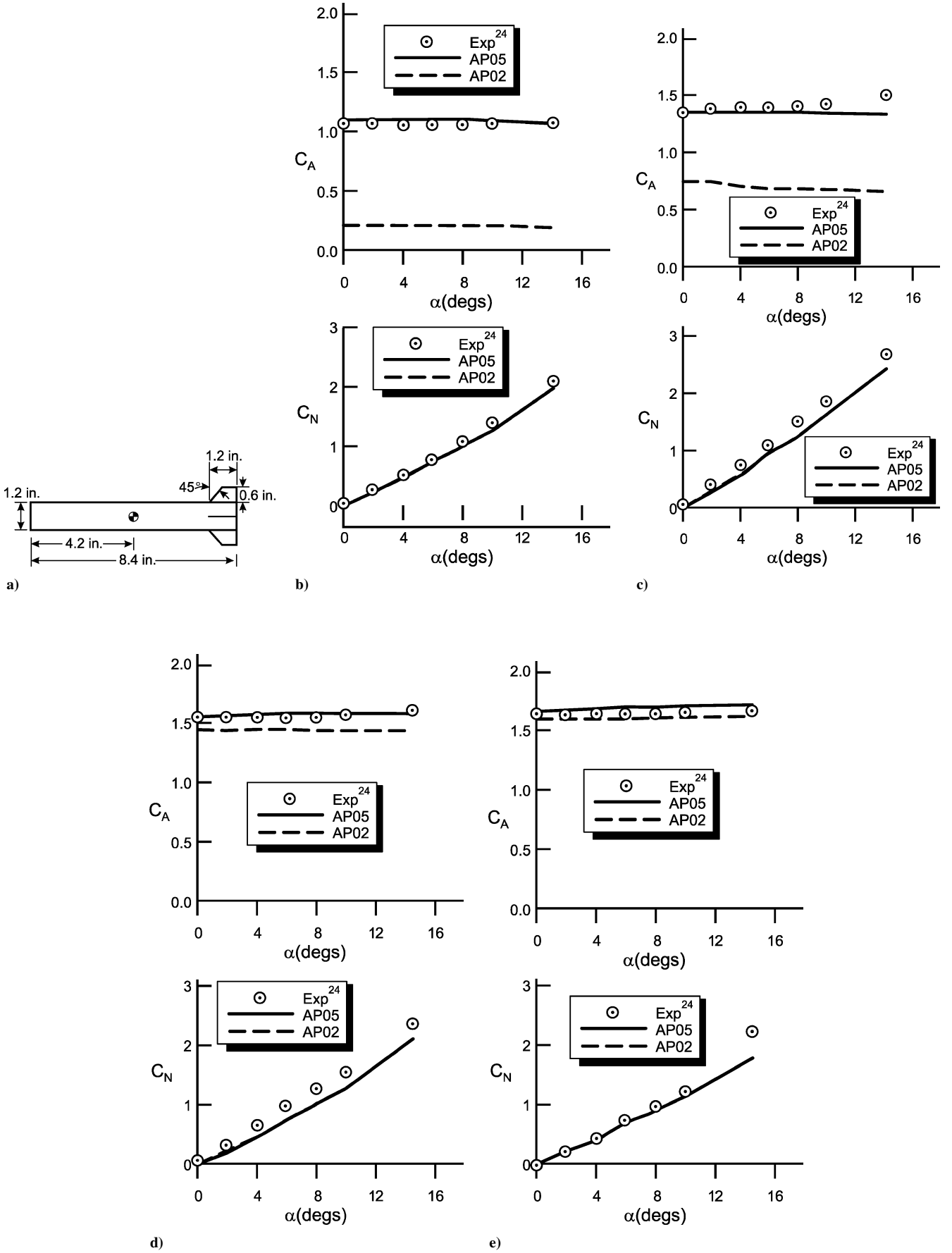

Fig. 9 Flat-faced cylinder with tail fins[24]: a) configuration; b) axial and normal force coefficient comparisons $M_\infty = 0.6$, $R_N = 4.4 \times 10^6$/ft, $\Delta M_{N_C} = 0.03$; c) axial and normal force coefficient comparisons $M_\infty = 1.0$, $R_N = 4.8 \times 10^6$/ft, $\Delta M_{N_C} = 0.055$; d) axial and normal force coefficient comparisons $M_\infty = 1.2$, $R_N = 4.8 \times 10^6$/ft, $\Delta M_{N_C} = 0.25$; and e) axial and normal force coefficient comparisons $M_\infty = 1.5$, $R_N = 4.8 \times 10^6$/ft, $\Delta M_{N_C} = 0.40$.

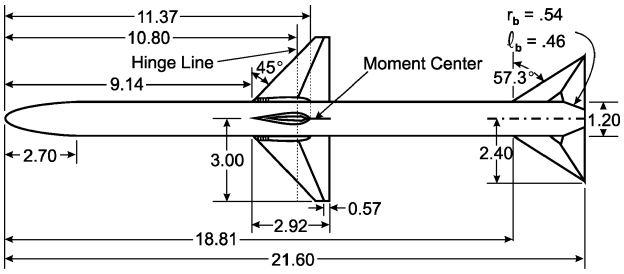

Fig. 10 Wing–body–tail configuration used in validation process (all dimensions in inches).

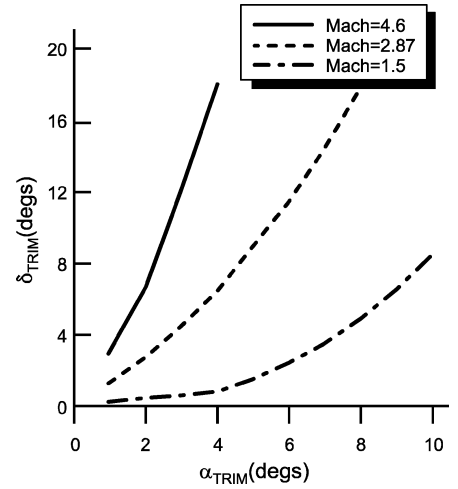

a)

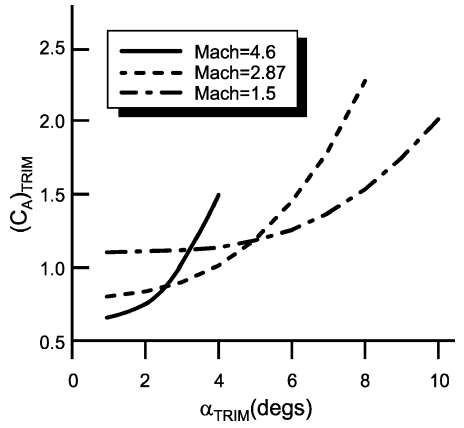

b)

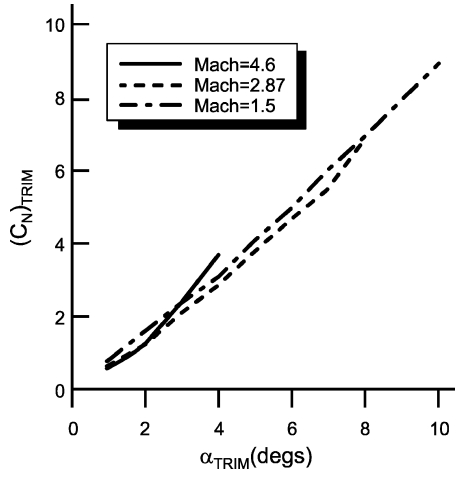

c)

Fig. 11 Wing–body–tail configuration (Fig. 10) at $\Phi = 0$ deg: a) control deflection vs α_{trim}, b) $(C_A)_{trim}$ vs α_{trim}, and c) $(C_N)_{trim}$ vs α_{trim}.

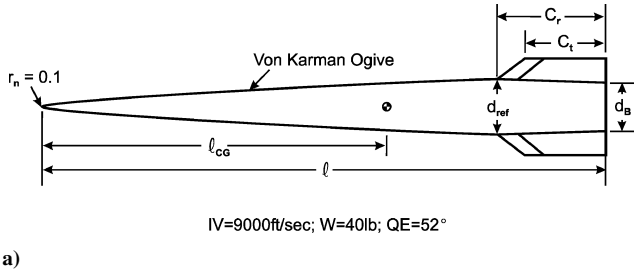

a)

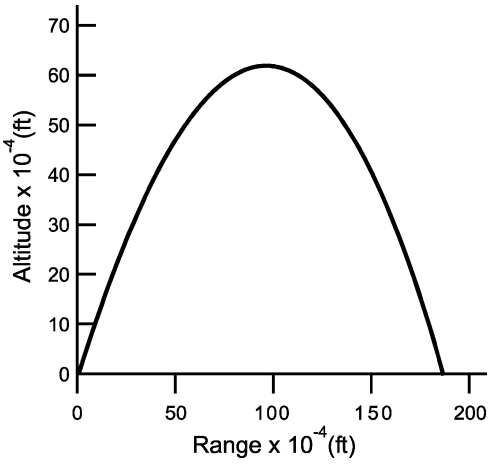

b)

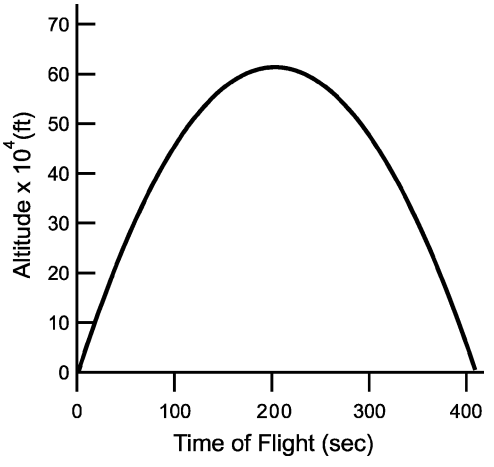

c)

Fig. 12 Long-range projectile: a) concept, b) altitude vs range, and c) altitude vs time of flight.

Increase in Altitude Limits Example Case

One example will be given to illustrate the new altitude limit increase from 2.5×10^5 ft to 1×10^6 ft. The example chosen is a concept similar to one being considered for an electromagnetic gun and is shown in Fig. 12a. The Fig. 12a configuration is very low drag and has a very high initial velocity. Figures. 12b and 12c show two of the plots available in AP05 including missile altitude vs missile horizontal position and missile altitude vs time of flight. The Fig. 12a configuration attains an altitude in excess of 600,000 ft, well above the limit of 250,000 ft in AP02.

Summary

A new version of the APC, AP05, has been developed. AP05 includes several new elements and improvements in accuracy compared to AP02. The new capabilities include three-fin aerodynamics, blunt trailing-edge fin effects on normal-force coefficient, increase in trajectory altitude capability, protuberance aerodynamic input options, user-defined boundary-layer transition option, and trim aerodynamics. Additional improvements in two-dimensional

base pressure coefficients, truncated fin leading-edge axial force, large truncated nose axial force, and small caliber weapons were obtained by developing new technology or refining existing technology in the AP02 code.

To validate AP05, approximately 50 different configurations were considered, which covered the overall flight regime, configuration geometry, and application requirements of AP05. It was found that AP05 gave improved accuracy over AP02 when compared to experimental data where new methods were incorporated in AP02 to form AP05. It was also found AP02 and AP05 continued to give similar accuracy on static and dynamic aerodynamics, for configurations that were not affected by the new elements of AP05. The many new features incorporated into AP05 made it much more robust than AP02. As such, it is believed AP05 is the most accurate and robust of the aerodynamic prediction codes produced to date.

References

[1]Moore, F. G., "Body Alone Aerodynamics of Guided and Unguided Projectiles at Subsonic, Transonic, and Supersonic Mach Numbers," U.S. Naval Surface Warfare Center, Rept. NWL TR-3796, Dahlgren, VA, Nov. 1972.

[2]Moore, F. G., and McKerley, C. W., "Aerodynamics of Guided and Unguided Weapons: Part I—Theory and Application," U.S. Naval Surface Warfare Center, Rept. NWL TR-3018, Dahlgren, VA, Dec. 1973.

[3]Moore, F. G. and Swanson, C., "Aerodynamics of Tactical Weapons to Mach Number 3 and Angle of Attack 15 Degrees: Part I—Theory and Application," U.S. Naval Surface Warfare Center, Rept. NSWCDL TR-3584, Dahlgren, VA, Feb. 1977.

[4]Devan, L., Mason, L., and Moore, F. G., "Aerodynamics of Tactical Weapons to Mach Number 8 and Angle-of-Attack 180 Degrees," AIAA Paper 82-0250, Jan. 1982.

[5]Moore, F. G., McInville, R. M., and Hymer, T. C., "An Improved Version of the Naval Surface Warfare Center Aeroprediction Code (AP93)," *Journal of Spacecraft and Rockets*, Vol. 31, No. 5, 1994, pp. 783–791.

[6]Moore, F. G., McInville, R. M., and Hymer, T. C., "The 1995 Version of the NSWC Aeroprediction Code: Part I—Summary of New Theoretical Methodology," U.S. Naval Surface Warfare Center, Rept. NSWCDD/TR-94/379, Dahlgren, VA, Feb. 1995.

[7]Moore, F. G., McInville, R. M., and Hymer, T. C., "The 1998 Version of the NSWC Aeroprediction Code: Part I—Summary of New Theoretical Methodology," U.S. Naval Surface Warfare Center, Rept. NSWCDD/TR-98/1, Dahlgren, VA, April 1998.

[8]Moore, F. G., and Hymer, T. C., "The 2002 Version of the Aeroprediction Code: Part I—Summary of New Theoretical Methodology," U.S. Naval Surface Warfare Center, Rept. NSWCDD/TR-01/108, Dahlgren, VA, March 2002.

[9]Moore, F. G., and Hymer, T. C., "The 2005 Version of the Aeroprediction Code: Part I—Summary of New Methodology," Aeroprediction, Inc., API Rept. 1, King George, VA, Jan. 2004.

[10]Moore, F. G., McInville, R. M., and Robinson, D. I., "A Simplified Method for Predicting Aerodynamics of Multi-Fin Weapons," U.S. Naval Surface Warfare Center, Rept. NSWCDD/TR-99/19, Dahlgren, VA, March 1999.

[11]Moore, F. G., and Hymer, T. C., "An Approximate Method to Estimate Wing Trailing-Edge Bluntness Effects on Normal Force," AIAA Paper 2004-16, Jan. 2004.

[12]Chapman, D. R., and Kester, R. H., "Effect of Trailing-Edge Thickness on Lift at Supersonic Speeds," NACA RM A52D17, July 1952.

[13]Jaeger, B. F., Luther, M. L., and Schroedter, G. M., "The Aerodynamic Characteristics at Supersonic Speeds of Blunt-Trailing-Edge Airfoils for the NOTS Small-Caliber Air-to-Air Folding-Fin Rocket," NAVORD Rept. 1287 (NOTS 357), Feb. 1951; also Rept. DTIC AD B954298.

[14]Hoerner, S. F., *Fluid Dynamics Drag,* Hoerner Fluid Dynamics, Brick Town, NJ,1965, pp. 3-12, 3-13.

[15]Morrow, J. D., "Measurements of the Effect of Trailing-Edge Thickness on the Zero-Lift Drag of Thin Low-Aspect-Ratio Wings," NACA TN 3550, Nov. 1955.

[16]Wu, J. M., and Aoyoma, M., "Transonic Flow-Fluid Calculation Around Ogive Cylinders by Nonlinear-Linear Stretching Method," U.S. Army Missile Command, TR RD-70-12, Huntsville, AL, April 1970.

[17]Moore, F. G., *Approximate Methods for Weapon Aerodynamics,* Vol. 186, Progress in Astronautics and Aeronautics, AIAA, Reston, VA, 2000, Chaps. 3 and 5.

[18]Rogers, R. M., and Butler, C. M., "Aerodynamic Characteristics of Several Bluff Body Configurations at Subsonic and Transonic Mach Numbers," Rept. AFATL TR-72-25, Eglin AFB, FL, Feb. 1972.

[19]Minzner, R. A., Champion, K. S. W., and Pond, H. L., "The ARDC Model Atmosphere," Rept. AFCRC-TR-59-267, 1959; also DTIC AD 229482.

[20]Hathaway, W. H., Kruggel, B., Abate, G., Winchenbach, G., and Krieger, J., "Aeroballistic Range Tests of Missile Configurations with Non-circular Cross Sections," Munitions Directorate, Rept. AFRL-MN-EG-TR-2001-7082, U.S. Air Force Research Lab., Eglin AFB, FL, Sept. 2001.

[21]McKinney, R. L., "Longitudinal Stability and Control Characteristics of an Air-to-Air Missile Configuration at Mach Numbers 2.3 and 4.6 and Angles of Attack -45 to 90°," NASA TM X-846, 1972.

[22]Monta, W. J., "Supersonic Aerodynamic Characteristics of a Sparrow III Type Missile Model with Wing Controls and Comparison with Existing Tail-Control Results," NASA TP 1078, Nov. 1977.

[23]"Equations, Tables, and Charts for Compressible Flow," NACA Rept. 1135, 1953.

[24]Rogers, R. M., and Butler, C. M., "Aerodynamic Characteristics of Several Fluff Body Configurations at Subsonic and Transonic Mach Numbers," U.S. Air Force Armament Lab., Rept. AFATL-TR-72-25, Eglin AFB, FL, Feb. 1972.

M. Miller
Associate Editor